

Impact of amorphization on the electronic properties of Zn–Ir–O systems

This content has been downloaded from IOPscience. Please scroll down to see the full text.

2016 J. Phys.: Condens. Matter 28 345502

(<http://iopscience.iop.org/0953-8984/28/34/345502>)

View [the table of contents for this issue](#), or go to the [journal homepage](#) for more

Download details:

IP Address: 131.111.184.102

This content was downloaded on 17/08/2017 at 15:54

Please note that [terms and conditions apply](#).

You may also be interested in:

[P-type transparent conducting oxides](#)

Kelvin H L Zhang, Kai Xi, Mark G Blamire et al.

[GGA + U study of native point defects in ZnRh₂O₄](#)

O Volnianska and P Boguslawski

[Multi-component transparent conducting oxides: progress in materials modelling](#)

Aron Walsh, Juarez L F Da Silva and Su-Huai Wei

[Comparison of the electronic structure of amorphous versus crystalline indium gallium zinc oxide semiconductor: structure, tail states and strain effects](#)

A de Jamblinne de Meux, G Pourtois, J Genoe et al.

[Electronic structure of transparent oxides with the Tran–Blaha modified Becke–Johnson potential](#)

H Dixit, R Saniz, S Cottenier et al.

[Assessing the potential of Mg-doped Cr₂O₃ as a novel p-type transparent conducting oxide](#)

Aoife B Kehoe, Elisabetta Arca, David O Scanlon et al.

[P-type zinc oxide spinels: application to transparent conductors and spintronics](#)

Maria Stoica and Cynthia S Lo

[First-Principle Studies on Conductive Behaviors of P-Type ZnO Codoped by N and B](#)

Li Ping, Deng Sheng-Hua, Zhang Xue-Yong et al.

[Semiconducting transition metal oxides](#)

Stephan Lany

Impact of amorphization on the electronic properties of Zn–Ir–O systems

David Muñoz Ramo¹ and Paul D Bristowe²

¹ Department of Chemistry, University of Cambridge, Lensfield Road, Cambridge CB2 1EW, UK

² Department of Materials Science and Metallurgy, University of Cambridge, 27 Charles Babbage Road, Cambridge CB3 0FS, UK

E-mail: dm586@cam.ac.uk and pdb1000@cam.ac.uk

Received 16 March 2016, revised 23 May 2016

Accepted for publication 3 June 2016


Published 29 June 2016



Abstract

We analyze the geometry and electronic structure of a series of amorphous Zn–Ir–O systems using classical molecular dynamics followed by density functional theory taking into account two different charge states of Ir (+3 and +4). The structures obtained consist of a matrix of interconnected metal-oxygen polyhedra, with Zn adopting preferentially a coordination of 4 and Ir a mixture of coordinations between 4 and 6 that depend on the charge state of Ir and its concentration. The amorphous phases display reduced band gaps compared to crystalline ZnIr_2O_4 and exhibit localized states near the band edges, which harm their transparency and hole mobility. Increasing amounts of Ir in the Ir^{4+} phases decrease the band gap further while not altering it significantly in the Ir^{3+} phases. The results are consistent with recent transmittance and resistivity measurements.

Keywords: amorphous oxides, density functional theory, transparency, *p*-type conductivity

 Online supplementary data available from stacks.iop.org/JPhysCM/28/345502/mmedia


(Some figures may appear in colour only in the online journal)

1. Introduction

Transparent conducting oxides have become a staple of the optoelectronics industry, appearing in many everyday devices like light emitting diodes, flat panel displays or photovoltaic cells, among others. These materials display a useful combination of good electrical conductivity and transparency in the visible region of the electromagnetic spectrum [1–3]. The most well known examples correspond to the family of Zn- and In-based oxide semiconductors such as indium tin oxide or indium gallium zinc oxide, which display *n*-type electrical conductivity [4]. Progress in their *p*-type counterparts has been slower despite being essential for the development of *p*-*n* junctions, which would enable the design of transparent transistor devices. In this case, problems related to low hole mobilities of different candidate materials have been reported

[5, 6]. Nonetheless, several oxides like CuAl_2O_4 [7], ZnRh_2O_4 [8] or, more recently, ZnIr_2O_4 [9, 10] look promising and are being investigated in detail.

In addition to the combination of transparency and electrical conductivity, another key property from the point of view of device integration is the possibility of obtaining amorphous phases without too much harm to the optical and electrical properties of the material. This property is desired for the better homogeneity obtained in the material and the lower temperatures needed for its processing. In general, *n*-type transparent conducting oxides maintain their good electrical conductivity and transparency in the amorphous phase. The origin of this behaviour is the peculiar electronic structure of these oxides: in most of them, the bottom of the conduction band is mainly composed of contributions of *s* orbitals from the cations. Overlap between these orbitals is largely maintained in the amorphous phase thanks to their spherical symmetry, which conserves the large dispersion of the bottom of the conduction band and maintains low electron effective masses [11]. The situation is not so favorable in *p*-type oxides;

 Original content from this work may be used under the terms of the [Creative Commons Attribution 3.0 licence](https://creativecommons.org/licenses/by/3.0/). Any further distribution of this work must maintain attribution to the author(s) and the title of the work, journal citation and DOI.

in the most studied case, the delafossite CuAl_2O_4 , the hole mobility is severely reduced upon amorphization [7]. In this material, the top of the valence band is composed of a hybridization of $O\ p$ orbitals and $\text{Cu}\ d$ orbitals that are very sensitive to structural distortions.

Other classes of materials are currently being explored with the goal of achieving a technologically relevant p -type amorphous oxide. One of these classes is that of Zn spinels with d^6 transition metals like Co, Rh or Ir [7, 9]. In these spinels, the gap region is dominated by d - d orbital splitting of the d^6 metal, which is of the order of 2–3 eV. In addition, hole production to enable p -type conduction is favored in these systems by the abundance of Zn antisite defects in the lattice [12]. Several groups have attempted to grow thin films of these materials. Kamiya *et al* report the growth of ZnRh_2O_4 amorphous films, whose hole mobility is still high compared with the spinel phase, but transparency is harmed by optical transitions at 1 eV [8]. More recently, resistivity and spectroscopy measurements have been conducted on Zn–Ir–O amorphous films with Ir concentrations in the range 6.7–66.2 at.% [13, 14]. These studies indicate that hole conduction takes place through a variable range hopping mechanism which is thermally activated when the Ir concentration is between 16–45 at.%. In addition, it is observed that both the resistivity and the transmittance of the samples before annealing decrease with iridium concentration. These observations display similarities between this material and amorphous ZnRh_2O_4 , indicating that the mechanism governing transparency must lie in general electronic structure features of the Zn–(Co/Rh/Ir)–O systems.

In this paper, we focus our attention on the Zn–Ir–O case. This system has been studied with atomistic modelling methods in its ZnIr_2O_4 spinel structure. Scanlon *et al* [15] reported density functional theory (DFT) calculations using the HSE hybrid functional, where they reproduced the band gap of this oxide and observed a narrow bandwidth at the top of the valence band. Amini *et al* [16] found formation energies and localized levels for a collection of common defects in the spinel structure. We also addressed the ZnIr_2O_4 composition in a previous study where a combined DFT/classical molecular dynamics approach allowed us to design an amorphous model and calculate its electronic structure with the B3LYP hybrid functional [17]. There, we predicted that amorphization would harm both transparency and hole mobility. However, the influence of Ir/Zn ratio variations on the electronic structure, and therefore on the mechanisms that control hole conduction and transmittance of the system, was not studied. In addition, the oxidation state of Ir has to be considered. At ambient conditions, Ir-containing oxides are predominantly found with Ir in the +4 charge state. Well-known examples are IrO_2 , Ba_2IrO_4 or Sr_2IrO_4 . In this sense, the spinel ZnIr_2O_4 (with Ir in the +3 charge state) is an anomaly, and the reported difficulty in its thin film growth [9] suggests that this may be a metastable phase. Therefore, the possibility that amorphous Zn–Ir–O phases may be more stable with Ir in the +4 charge state instead of the +3 state must be considered.

In the present study we investigate the effect of variations in the Ir concentration and charge state on the electronic

structure and properties of amorphous Zn–Ir–O by using our combined simulation approach. We create models for amorphous phases considering different Ir/Zn proportions resulting in Ir concentrations in the range 14.3–31.6 at.%. The relative stability of systems where Ir is in the +3 or the +4 charge state is considered. We start by describing our atomistic modelling method and then present our results for the Ir^{3+} and Ir^{4+} phases. Finally, we look at the stability of the different charge states of Ir in our models before presenting our conclusions and relate them to existing experimental observations.

2. Computational method

Our models were developed combining several techniques. Here we provide a brief description of the procedure used; for a more detailed explanation, please refer to the supplementary information (stacks.iop.org/JPhysCM/28/345502/mmedia).

In the first step, we created large supercells (of about 10 000–12 000 atoms) of Zn–Ir–O systems with different proportions of Ir/Zn atoms and compensating O atoms to maintain supercell charge neutrality. For the Ir^{3+} models, we created the starting geometries by using a large ZnIr_2O_4 spinel supercell where atoms are substituted or removed at random lattice positions to account for the different proportions that we wanted to study. For the Ir^{4+} models, we followed the same procedure but the starting geometries were designed by creating a hypothetical Zn_2IrO_4 unit cell with the lattice parameters and atom coordinates of Sr_2IrO_4 which has been experimentally synthesised [18, 19]. The lattice parameters and atom coordinates of this unit cell were then relaxed using DFT. The geometry and electronic structure of this virtual material can be found in the supplementary information. Once we had our starting supercells, we performed a series of molecular dynamics calculations on them with classical interatomic potentials using the DL_POLY code [20]. The interatomic potentials were obtained after fitting to *ab initio* structural data of several Ir–Zn–O crystalline phases using the GULP code [21]. The supercells were first melted at 5000 K and equilibrated at constant pressure and temperature to ensure that the atoms lost memory of their initial positions, and the lattice parameters adjusted to the different chemical compositions. Then, these supercells were rapidly quenched at constant pressure to 300 K, at a rate of 0.08 K fs^{-1} , and equilibrated afterwards.

In the second step, we extracted a small model (100–120 atoms) from the large supercell obtained via the melt-and-quench process. This small model was refined using the Reverse Monte Carlo method with the RMC++ code [22–24] so that it reflected the average properties of the large model. In the Monte Carlo procedure, convergence was achieved by ensuring maximum correspondence between the radial distribution function of the small model and that of the large supercell.

The final step consisted of calculating the electronic structure of the small cell obtained with the Reverse Monte Carlo method using DFT. The B3LYP hybrid functional, as implemented in the CRYSTAL09 code [25] was selected as it provides values for the band gap and the relative positions

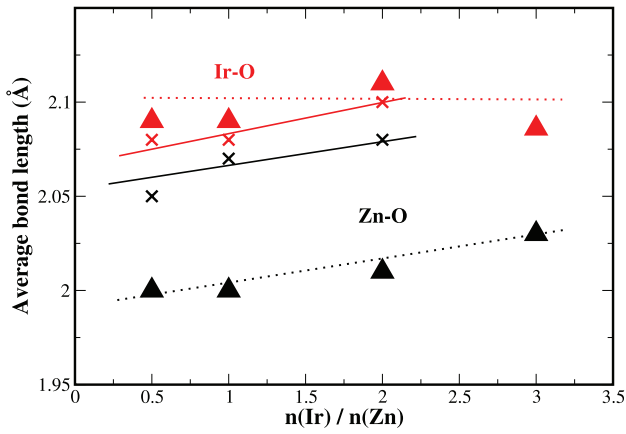


Figure 1. Average Ir–O and Zn–O nearest neighbour distances in the Ir^{3+} and Ir^{4+} models with respect to the $n(\text{Ir})/n(\text{Zn})$ ratio. Triangles and crosses correspond to Ir^{3+} and Ir^{4+} models, respectively. Zn–O distances are shown in black, while Ir–O distances are in red. Lines are drawn as a guide to the eye for each set of distances, distinguishing Ir^{3+} results (dashed lines) from Ir^{4+} results (solid lines).

of the O p , Ir d and Zn d bands of ZnIr_2O_4 in good agreement with experiment [17]. Spin polarization was used in all the calculations. Supercell size effects were considered to be not important for the purposes of the qualitative analysis of the electronic structure performed in this work (see the supplementary information for more details). We also performed a final geometry optimization of the supercell models using this functional to obtain a more accurate structure and remove possible structural artefacts introduced by the RMC method. Spin–orbit coupling effects were not included as they only have a minor effect on the band gap of bulk ZnIr_2O_4 [26].

With this approach, we created models at different Ir atom percentages ($n(\text{Ir})$). For the Ir^{3+} case, we consider $n(\text{Ir}) = 15.38$ at.%, 22.22 at.%, 28.57 at.% and 31.57 at.%, corresponding to systems with stoichiometries $\text{Zn}_4\text{Ir}_2\text{O}_7$, $\text{Zn}_2\text{Ir}_2\text{O}_5$, ZnIr_2O_4 and $\text{Zn}_2\text{Ir}_6\text{O}_{11}$. For the Ir^{4+} case, the systems studied are $n(\text{Ir}) = 14.29$ at.% (Zn_2IrO_4), 20 at.% (ZnIrO_3) and 25 at.% (ZnIr_2O_5).

3. Results

We proceed to describe in detail the features obtained for each model presented in the previous section. We divide our results into two subsections, one discussing the structural features of the amorphous phases obtained, and another one describing the electronic structure resulting from the geometries and compositions considered.

3.1. Structure of the amorphous phases

Figures 1 (average bond lengths) and 2 (average metal–oxygen coordinations) summarize the structural features of the different models considered in this study. Coordinations were calculated by integrating the corresponding partial radial distribution function up to its first minimum for each supercell. In the Ir^{3+} models, the average Ir–O bond length is about

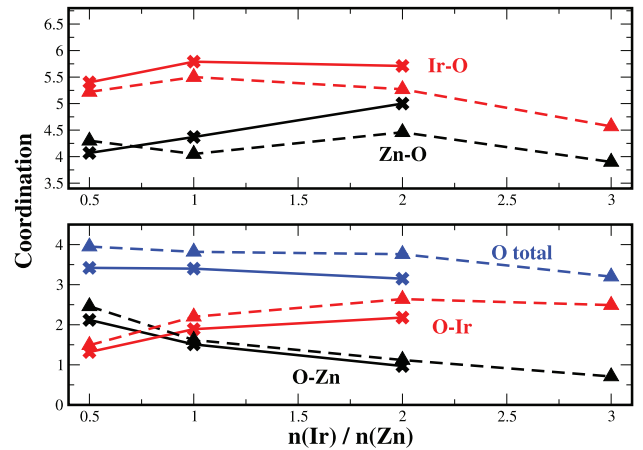


Figure 2. Top: average Ir–O and Zn–O nearest neighbour coordination with respect to the $n(\text{Ir})/n(\text{Zn})$ ratio in the Ir^{3+} and Ir^{4+} models. Bottom: average O–Ir and O–Zn coordination. Triangles joined by dashed lines correspond to the Ir^{3+} models, and crosses joined by solid lines correspond to the Ir^{4+} models.

0.1 Å larger than the average Zn–O bond length. Both bond lengths show very little dependence on the Ir/Zn ratio. The Ir–O bonds have, on average, similar length to that of their analogues in the spinel structure, while the Zn–O bonds are about 0.05 Å shorter.

Ir–O and Zn–O coordinations also exhibit small changes with Ir/Zn ratio. The Ir–O average coordination increases from about 5.2 at $n(\text{Ir}) = 15.38$ at.% to about 5.5 at $n(\text{Ir}) = 22.22$ at.%. Then, it decreases until reaching a value of about 4.6 at $n(\text{Ir}) = 31.57$ at.%. The Zn–O coordination oscillates between about 4.0 and 4.5 in the same composition interval (see figure 2). The oxygen–metal coordination is more sensitive to the Ir/Zn ratio. In the O–Ir case, it evolves from about 1.4 at $n(\text{Ir}) = 15.38$ at.% to about 2.7 at $n(\text{Ir}) = 31.57$ at.%. In the O–Zn case, it decreases from about 2.5 to about 0.5 in the same interval. The total O coordination value decreases very slightly with increasing Ir amount in the supercell. These trends in oxygen–metal coordination show that Ir atoms become progressively interlinked while Zn atoms become progressively isolated as the concentration of Ir in the supercell increases. This leads to an increase in the number of edge-linked IrO_x polyhedra, although a large number of corner-linked polyhedra is still present for all Ir/Zn ratios considered.

We now analyze the results obtained for the Ir^{4+} models. In comparison with the Ir^{3+} models, the Ir–O average bond lengths tend to have slightly smaller values, as can be observed from figure 1, while the Zn–O bond lengths tend to be slightly larger. Average coordinations in the Ir^{4+} models are displayed in figure 2. The average Ir–O coordination number tends to be larger than in the Ir^{3+} , although it follows the same trend: increasing amount of Ir leading to a larger average coordination until reaching a peak value. This value never reaches 6, which means that there is still a significant number of undercoordinated Ir atoms. The Zn–O coordination number shows similar trends, i.e. an increase directly related to the amount of Ir but with slightly larger numbers than in the Ir^{3+} models. Values are above 4 in all cases, which indicates the presence of many overcoordinated Zn atoms.

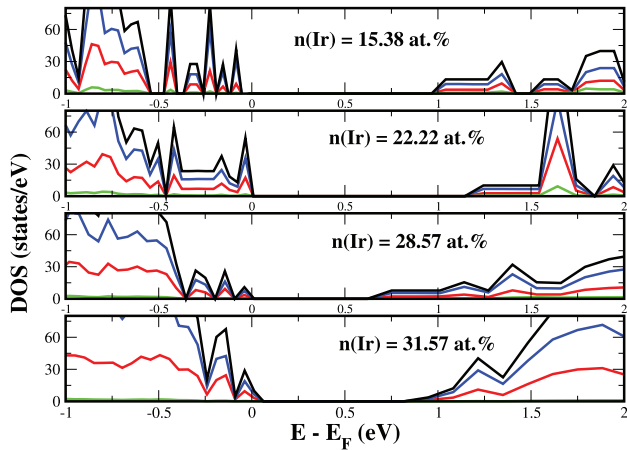


Figure 3. DOS of amorphous Ir–Zn–O phases (with Ir³⁺) at different Ir concentrations. Total DOS is represented by black lines. Red, green and blue lines correspond to O, Zn and Ir states, respectively. The Fermi level E_F is shifted to zero.

Oxygen-metal coordinations are, in general, smaller in the Ir⁴⁺ models than in the Ir³⁺ models, as shown in figure 2. Like in the Ir³⁺ case, total O coordination slowly decreases with increasing amount of Ir in the supercell. In the O–Ir case, the coordination numbers are smaller by about 0.3–0.5 and range from 1.3 at low Ir concentration to 2.0 at high Ir concentration. This indicates that edge-sharing IrO_x polyhedra are less abundant in the Ir⁴⁺ models and there are more nonlinking O atoms. For O–Zn coordination, the reduction is about 0.1–0.3 with coordination number decreasing from about 2.0 at low Ir concentrations to about 1.0 at high concentrations. This result corresponds to the progressive linking of the ZnO_x polyhedra in the structure as the concentration of Zn increases.

3.2. Electronic structure

The influence of amorphization on the electronic structure of the different Zn–Ir–O models has been studied by calculating the electronic density of states (DOS) for the small supercells obtained with the reverse Monte Carlo procedure. Inspection of the DOS in the gap region at different Ir concentrations (see figure 3) shows that amorphization leads to dramatic changes in the electronic structure of the Zn–Ir–O system. For the Ir³⁺ models, we find a large reduction in the band gap compared to that of spinel ZnIr₂O₄ (about 3.0 eV using B3LYP [17]), which will lead to a reduced transparency of the amorphous phase. This reduction is found at all Ir concentrations. In addition, the band edges are populated with localized levels mainly of Ir *d* nature, corresponding to undercoordinated Ir atoms and distorted IrO₆ polyhedra. The bands corresponding to these levels are narrow, with dispersions between 0.1 and 0.3 eV (see the supplementary information for band diagrams of all the supercells considered). Such narrow bands at the top of the valence band are indicative of large hole effective masses and decreased hole conductivities in these systems. The value of the band gap does not follow a clear trend with respect to Ir concentration and deviates from the mean by about 0.2 eV.

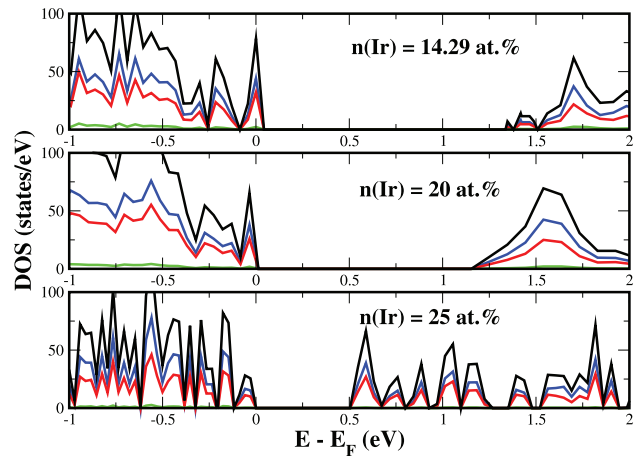


Figure 4. DOS of the different Ir⁴⁺ models considered. Total DOS is represented by black lines. Red, green and blue lines correspond to O, Zn and Ir states, respectively. The Fermi level E_F is shifted to zero.

The Ir⁴⁺ models also have small band gaps and an abundance of localized states near the band edges (see figure 4), which will also lead to reduced hole conductivities. However, the band gap depends more strongly on the Ir/Zn ratio: it evolves from 1.4 eV at low Ir concentration to about 0.5 eV at high concentration. At the highest Ir concentration considered, we also observe a decrease in the number of localized edge states due to the improved overlap between Ir *d* orbitals induced by the decrease of the average Ir–Ir distance. The presence of a band gap in the Ir⁴⁺ models is remarkable, as the Ir⁴⁺ binary oxide (IrO₂) is metallic. One may assume that the presence of Zn in the system induces the opening of the band gap, as ZnO is a semiconductor with a band gap of about 3 eV. However, an inspection of the states in the valence and conduction bands shows that they are composed mainly of Ir *d* with minor contributions from O *p* states. Zn states are not present in this region of the DOS. Therefore, the band gap opening must be produced by geometric distortions in the local environment of the IrO_x polyhedra.

We now examine in more detail the source of the localized states in the gap region. Figure 5 shows the relative contribution from fourfold- (4C), fivefold- (5C) and sixfold-coordinated (6C) Ir atoms to the states in the gap region of each model (red and green symbols). These contributions are compared to the relative number of Ir atoms with different coordinations in each DFT supercell (black symbols). We start with the Ir³⁺ case. The region near the valence band maximum (red symbols) shows similar contributions from 5C and 6C Ir atoms in the 15.38 at.%, 22.22 at.% and 28.57 at.% compositions. However, in the 31.57 at.% composition we find that 6C contributions become very small with respect to the other contributions. The contributions from 4C Ir atoms increase with the amount of Ir in the cell until reaching a similar proportion to that from 5C atoms. Comparison with the relative abundance of different coordinations in the supercell (black symbols) shows that 5C Ir atoms contribute less than expected to the upper valence band DOS, while the 4C and 6C atoms contribute more. The opposite is observed in the upper gap region. There, the 5C-induced states

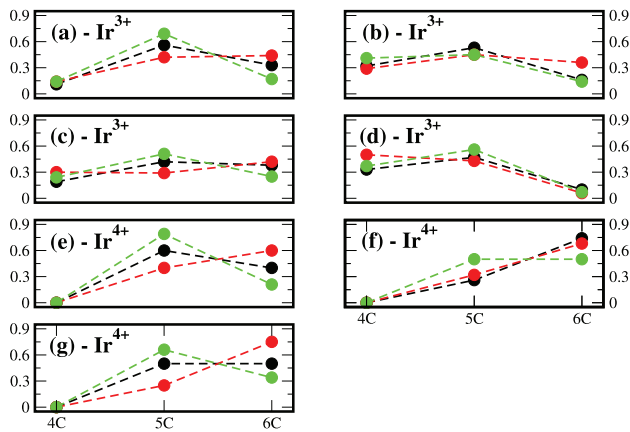


Figure 5. Relative contribution to the localized states in the gap region from 4C, 5C and 6C Ir atoms. Contributions from states near the valence band maximum are represented with red symbols whereas contributions from states near the conduction band region are represented with green symbols. The ratio of 4C, 5C and 6C Ir atoms in each model is included for comparison (black symbols). Lines are drawn to guide the eye. Each graph corresponds to a different Ir–Zn–O model: (a) $n(\text{Ir}) = 15.38$ at.% (Ir^{3+}); (b) $n(\text{Ir}) = 22.22$ at.% (Ir^{3+}); (c) $n(\text{Ir}) = 28.57$ at.% (Ir^{3+}); (d) $n(\text{Ir}) = 31.57$ at.% (Ir^{3+}); (e) $n(\text{Ir}) = 14.29$ at.% (Ir^{4+}); (f) $n(\text{Ir}) = 20.0$ at.% (Ir^{4+}); (g) $n(\text{Ir}) = 25.0$ at.% (Ir^{4+}).

have higher abundances than the 4C and 6C-induced states, and their relative contribution is equal to or higher than the abundance of 5C Ir atoms in the supercells. This indicates that the Ir d states originating from fourfold and sixfold coordination environments are more stabilized than the d states originating from fivefold coordination environments and tend to populate the upper valence band, while the less stable 5C-induced states increase their energy and produce most of the localized states in the lower conduction band region. We see a similar behaviour in the Ir^{4+} models, although there are no 4C Ir atoms in the supercells considered, so they do not play a role in the production of localized states in the gap region. In addition, we observe an increased Ir 6C contribution in the upper valence band region in comparison with the Ir^{3+} results. This contribution reaches a maximum at the highest Ir concentration as a result of the increased interlinking of IrO_6 octahedra in the amorphous matrix.

Lastly we consider the relative stability of the Ir^{3+} and Ir^{4+} amorphous phases having the same Ir/Zn ratio. To do this we evaluate the energy at B3LYP level required to transform each Ir^{3+} model obtained by RMC into the corresponding Ir^{4+} model by the addition of oxygen. We take half the energy of the O_2 molecule as the energy for atomic oxygen and consider oxygen-rich conditions for the reaction. The energy for this oxidation process is shown in table 1 for three different Ir/Zn ratios. In all cases, oxidation to the Ir^{4+} phase is favored for the conditions considered.

4. Discussion and conclusions

Using a combination of classical molecular dynamics and density functional theory we have developed atomistic models for amorphous Zn–Ir–O phases with Ir concentrations between

Table 1. Energy per Ir atom (in eV) for the oxidation of each Ir^{3+} model into the corresponding Ir^{4+} model.

Ir/Zn ratio	ΔH
0.5	−0.84
1.0	−1.10
2.0	−0.76

14.3 at.% and 31.6 at.%, considering Ir in the +3 and +4 charge states. For both the Ir^{3+} and Ir^{4+} phases, we obtain structures where Ir atoms in different coordinations to oxygen can be found, with proportions that depend on the amount of Ir in the system. These coordination polyhedra are linked by both edges and corners to each other, in contrast to spinel ZnIr_2O_4 , where the octahedra are exclusively linked through their edges. Zn–O coordination is also dependent on the Ir concentration, with ZnO_4 tetrahedra dominating at large Ir concentrations and higher order coordinations appearing at small concentrations. The partial loss of edge-linked IrO_x polyhedra and changes in Ir coordination induce a decrease in the band gap of the amorphous phases. This effect is not systematically dependent on Ir concentration in the Ir^{3+} models, while in the Ir^{4+} models we find a clear decrease in the band gap as the amount of Ir in the model increases. The energetics of oxidation indicates that Ir^{4+} phases are more stable than Ir^{3+} phases.

Finally our results can be compared to recent structural, electrical and optical measurements made on various Zn–Ir–O thin film systems prepared by reactive DC magnetron sputtering [13, 14]. The structural observations indicate that the thin films are x-ray amorphous without the presence of crystalline oxides such as ZnO or ZnIr_2O_4 although after annealing nanocrystallites of IrO_2 form at high Ir concentrations (61.7 at.%). The structural models considered in the present study are consistent with these observations and furthermore predict that the +4 oxidation state of Ir is preferred over the +3 state which may partially explain the absence of ZnIr_2O_4 . The transmittance and resistivity measurements indicate that both these quantities decrease with increasing Ir concentration in the thin films which again is consistent with the present calculations which show a progressive decrease in band gap (resulting from the presence of localised band edge states) with Ir concentration when Ir is in the +4 charge state. Further calculations at high Ir concentrations (>50 at.%) would be required to determine the conditions necessary to nucleate IrO_2 and what effect that has on the electronic structure of the material.

Acknowledgments

Financial support for this work is provided by the European Commission through contract No.NMP3-LA-2010-246334 (ORAMA). We acknowledge computational support from the UK national high performance computing service ARCHER, for which access was obtained via the UKCP consortium and funded by EPSRC grant EP/K014560/1. All protocols and input parameters for performing the calculations are available in the publication or supplementary information.

References

- [1] Ohta H, Kawamura K-H, Hirano M, Sarukura N and Hosono H 2000 *Appl. Phys. Lett.* **77** 475
- [2] Thomas G 1997 *Nature* **389** 907
- [3] Ellmer K 2012 *Nat. Photon.* **6** 809
- [4] Fortunato E, Ginley D, Hosono H and Paine D C 2007 *MRS Bull.* **32** 242
- [5] Tsukazaki A *et al* 2005 *Nat. Mater.* **4** 42
- [6] Jiao S J, ZHANG Z Z, Lu Y M, Shen D Z, Yao B, Zhang B, Li H, Zhao D X, Fan X W and Tang Z K 2006 *Appl. Phys. Lett.* **88** 031911
- [7] Narushima S, Mizoguchi H, Shimizu K, Ueda K, Ohta H, Hirano M, Kamiya T and Hosono H 2003 *Adv. Mater.* **15** 1409
- [8] Kamiya T, Narushima S, Mizoguchi H, Shimizu K, Ueda K, Ohta H, Hirano M and Hosono H 2005 *Adv. Funct. Mater.* **15** 968
- [9] Dekkers M, Rijnders G and Blank D H A 2007 *Appl. Phys. Lett.* **90** 021903
- [10] Grochowski J, Kaminska E, Piotrowska A, Dynowska E, Dluzewski P, Dyczewski J, Szczepanska A and Kazmierczak P 2012 *Phys. Status Solidi c* **9** 1504
- [11] Walsh A, Da Silva J L F and Wei S-H 2011 *J. Phys.: Condens. Matter* **23** 334210
- [12] Paudel T R, Zakutayev A, Lany S, d'Avezac M and Zunger A 2011 *Adv. Funct. Mater.* **21** 4493
- [13] Zubkins M, Kalendarev R, Gabrusenoks J, Vilnis K, Azens A and Purans J 2014 *Phys. Status Solidi c* **11** 1493
- [14] Zubkins M, Kalendarev R, Gabrusenoks J, Smits K, Kundzins K, Vilnis K, Azens A and Purans J 2015 *IOP Conf. Ser. Mater. Sci. Eng.* **77** 012035
- [15] Scanlon D O and Watson G W 2011 *Phys. Chem. Chem. Phys.* **13** 9667
- [16] Amini M N, Dixit H, Saniz R, Lamoen D and Partoens B 2014 *Phys. Chem. Chem. Phys.* **16** 2588
- [17] Muñoz Ramo D and Bristowe P D 2014 *J. Chem. Phys.* **141** 084704
- [18] Crawford M K, Subramanian M A, Harlow R L, Fernandez-Baca J A, Wang Z R and Johnston D C 1994 *Phys. Rev. B* **49** 9198
- [19] Moretti Sala M *et al* 2014 *Phys. Rev. B* **90** 085126
- [20] Smith W and Todorov I T 2006 *Mol. Simul.* **32** 935
- [21] Gale J and Rohl A L 2003 *Mol. Simul.* **29** 291
- [22] McGreevy R L and Pusztai L 1988 *Mol. Simul.* **1** 359
- [23] Keen D A and McGreevy R L 1990 *Nature* **344** 423
- [24] Gereben O, Jovari P, Temleitner L and Pusztai L 2007 *J. Optoelectron. Adv. Mater.* **9** 3021
- [25] Dovesi R *et al* 2009 *CRYSTAL09 User's Manual* (University of Torino)
- [26] Singh N and Schwingenschlögl U 2013 *Europhys. Lett.* **104** 37002